**Open Access** **Baghdad Science Journal** **P-ISSN: 2078-8665**
**Published Online First: July 2021** **2022, 19(1): 105-120** **E-ISSN: 2411-7986**

DOI: http://dx.doi.org/10.21123/bsj.2022.19.1.0105

# Theoretical and Experimental Study of Corrosion Behavior of Carbon Steel Surface in 3.5% NaCl and 0.5 M HCl with Different Concentrations of Quinolin-2-One Derivative

***Rehab Majed Kubba**** ***Mustafa Alaa Mohammed***

Department of Chemistry, College of Science, University of Baghdad, Baghdad, Iraq.
*Correspond author: Rehab_mmr_kb@yahoo.com* , Mustafa.alaa602@yahoo.com
*ORCID ID: https://orcid.org/0000-0003-4855-7871*, https://orcid.org/0000-0001-7575-3558

Received 4/2/2020, Accepted 16/6/2020, Published Online First 20/7/2021, Published 1/2/2022



## Abstract:

A theoretical and protection study was conducted of the corrosion behavior of carbon steel surface with different concentrations of the derivative (Quinolin-2-one), namely 7-Ethyl-4-methyl-1-[(4-nitro-benzylidene)-amino]-1H-quinolin-2-one (EMNQ2O). Theoretically, Density Functional Theory (DFT) of B3LYP/ 6-311++G/ 2d, 2p level was carried out to calculate the geometrical structure, physical properties and chemical inhibition chemical parameters, with the local reactivity in order to predict both the reactive centers and to know the possible sites of nucleophilic and electrophilic attacks, in vacuum and two solvents (DMSO and $H_2O$), all at the equilibrium geometry. Experimentally, the inhibition efficiencies (%IE) in (3.5% NaCl) and (0.5M HCl) solutions were studied using potentiometric polarization measurements. The results revealed that the (%IE) in the salty solution (94.98%) is greater than that in the acidic solution (81.40%). The thermodynamic parameters obtained, supported the physical adsorption mechanism and the adsorption followed the Langmuir adsorption isotherm. The surface changes of the carbon steel were studied using SEM (Scanning Electron Microscopy) and AFM (Atomic Force Microscopy) techniques.

**Keywords:** Corrosion Inhibition, DFT, Quinolin, Thermodynamic parameters.

## Introduction:

Corrosion inhibitors are chemicals substances that interact with a metal surface or environments to which the metal surface is exposed and act to protect the metal from corrosion. [1] Most organic compounds having heterogeneous atoms (Nitrogen, Oxygen, Sulfur) in their aromatic composition have been successfully used as corrosion inhibitors [2]. Often high heterogeneous organic compounds and the density of electrons on heterogeneous atoms usually have a tendency to resist corrosion. Quantitative chemical calculations were used to study the reaction mechanism and to solve chemical mystery [3-6]. This is a useful approach to investigate the mechanism of the reaction molecule inhibitor and the metal surface. The structural and electronic parameters of the inhibitor molecule can be obtained by theoretical calculations using the computational methodologies of quantum chemistry. It is generally known that quinoline derivatives have a variety of pharmacological and biological activities, such as immunomodulatory, anti-malarial and anti-bacterial activity [7-8]. Numerous reports have been presented in the literature on the use of quinoline and some of its derivatives as corrosion inhibitors in various media [9-13]. In this search, it has been focused on the Quinolin-2-one derivative, a heterocyclic entity and pharmacologically important molecule.

The aim of this work is to study the inhibition efficiency of organic inhibitor (EMNQ2O) prepared by Luma SA. et. al. [14]; experimentally, in salty (3.5% NaCl) and acidic solutions using potentiostat method, and theoretically, the calculations of quantum chemical parameters were done in three media (vacuum, DMSO and water) using DFT of B3LYP/ 6-311++G/ 2d, 2p level theory and Gaussian 09 program.

## Materials and Methods:

### Preparation of carbon steel samples

Carbon steel's rod symbolized as (C45) having the following percentage of metallic

materials in composition (wt %): (0.122% C, 0.206% Si, 0.641% Mn, 0.016% P, 0.031% S, 0.118% Cr, 0.02% Mo, 0.105% Ni, and 0.451% Cu) [3]. The rod is mechanically cut into pieces forming a cyclic specimen of carbon steel a with 1.6 cm diameter and 3 mm thickness, each one of these specimen has been refined with emery paper (silicon carbide SiC) in different grades (80, 150, 220, 320, 400, 1000, 1200 and 2000) grades, then washed with tap water, distilled water and recent degreased with acetone, washed again with deionizer water, finally the specimen hold in a desiccators after it is dried in room temperature.

## Preparation solution

### Blank salt solution

35gm of sodium chloride (NaCl) was dissolved in (100 mL) distal water; transferred the formative solution into (1L) volumetric flask, containing 2mL of dimethyl sulfoxide (DMSO). The volume of the solution was completed to (1L) by adding distilled water. Using 3.5% NaCl is the suitable chooses in this study in order to avoid some problems related to the ohmic drop.

### Blank acid solution

40 mL (0.5M) of HCl was diluted by distilled water to (1 liter) in a volumetric flask, after adding 2mL of solvent of dimethyl sulfoxide (DMSO).

### Preparation the salty solutions of 7-Ethyl-4methyl-1-[(4-nitro-benzlidene)-amino]-1H-quinolin-2-one (EMNQ2O)

Three concentrations of the EMNQ2O inhibitor (5,10, and 20)ppm have been prepared by dissolving (0.005, 0.01 and 0.02) gm, respectively in (2mL) of DMSO, then transferred each one to (1L) volumetric flask containing 35gm (3.5%) of NaCl dissolved in distilled water. The volume of each solution was completed to 1L with distilled water.

### Preparation the acidic solutions of 7-Ethyl-4methyl-1-[(4-nitro-benzlidene)-amino]-1H-quinolin-2-one (EMNQ2O)

Three concentrations of the EMNQ2O inhibitor (5, 10, and 20) ppm were prepared by dissolving (0.005, 0.01 and 0.02) gm., respectively in (2mL) DMSO, then transferred each one to (1L) volumetric flask containing (40mL) HCl. The volume for each solution has been completed to (1L) with distilled water.

## Electrochemical measurements

### Potentiostatic polarization study

The potentiostat set up including host computer, Mat lab (Germany, 2000), magnetic stirrer, thermostat, potentiostat, and galvanostat. The main part of the apparatus is the corrosion cell; it's made of Pyrex with 1L capacity. This cell consists of two bowls external and internal. Three electrodes are mainly present in the electrochemical corrosion cell, carbon steel specimen having $1cm^2$ surface area has been represented as a working electrode that is used to determine the working electrode potential due to another electrode namely reference electrode was putting in a close to the working electrode. The reference electrode was s (Ag/AgCl, 3.0M KCl). The last electrode is a platinum auxiliary electrode having (10cm) length. The starting step has been represented by immersing the working electrode in the test solution for a period of (15 minute), to establish the potential of the open-circuit stable state ($E_{ocp}$). This possibility has been observed to start electrochemical measurements in the range of ±200 (mV). All tests have been conducted at (293, 303, 313 and 323) K.

## Results and Discussion:

### Quantum chemical calculations

The structural nature of the organic inhibitors and their inhibition mechanism were described by density functional theory (DFT). The inhibition efficiencies of compound (EMNQ2O) was investigated by the theoretical corrosion inhibition parameters such as energy of the highest occupied molecular orbital ($E_{HOMO}$) and energy of the lowest unoccupied molecular orbital ($E_{LUMO}$), energy gap ($E_{gap}$) between $E_{HOMO}$ and $E_{LUMO}$, dipole moment ($\mu$), electronegativity ($\chi$), electron affinity (A), global hardness ($\eta$), softness ($\sigma$), ionization energy (IE), global electrophilicity ($\omega$), the fraction of electrons transferred ($\Delta N$) and the total energy ($E_{tot}$) [15].

### The Molecular geometry

The organic inhibitors compound was built in two dimensions structure using Chem-Draw of Mopac program, (Fig. 1a). Gaussian 09 packages [16] were carried out for calculating the fully optimized structure in vacuum, using quantum mechanical method of DFT (Density Functional Theory) of Becke's three-parameter of Lee, Yang and Parr (B3LYP) with 6-311++G/ (2d, 2p) level of theory [17-19] (Fig. 1b). In addition to vacuum, the equilibrium geometry was calculated in two solvents (DMSO and $H_2O$).

Baghdad Science Journal
P-ISSN: 2078-8665
E-ISSN: 2411-7986

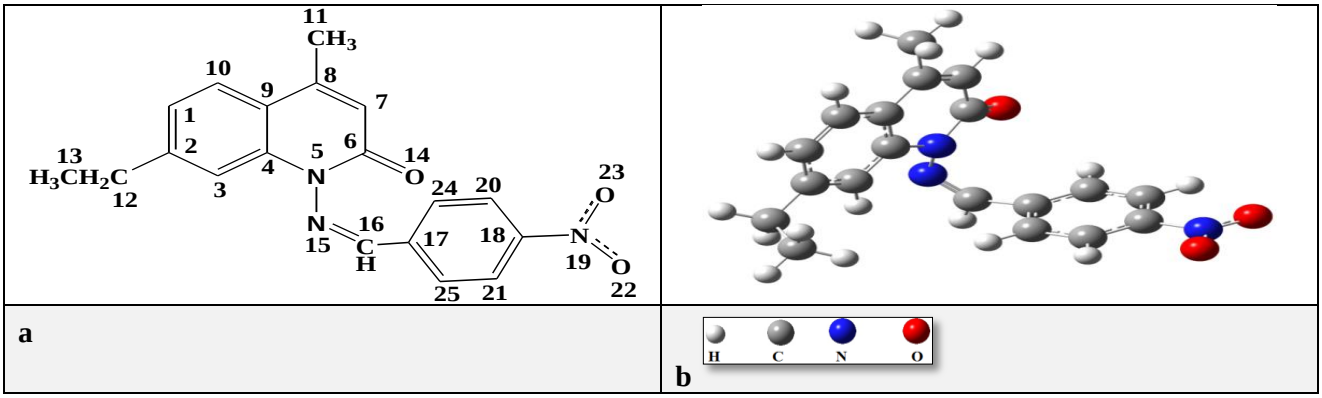


**Figure 1. a. Two dimensions structure of (7-ethyl-4-methyl-1-[(4-nitro-benzylidene)-amino]-1H-quinolin-2-one (EMNQ2O)) with the numbering of atoms. b. Three dimensions optimize structure of EMNQ2O inhibitor calculated by DFT method.**

Table 1 displays the geometrical structure details of EMNQ2O compound such as bond lengths, bond angels and dihedral angles which were calculated in vacuum and two solvents (DMSO, and $H_2O$) using DFT method. The optimized geometrical structure is the same in the three media (vacuum, DMSO, and $H_2O$). Table 1 shows that in EMNQ2O compound, the C12-C13 owns the longest bond length of (1.515 Å), and the C11-H26 bond is the shortest bond with (1.096 Å) length. The values of the dihedral angles (cis & trans) indicate non planarity of the compound within $C_1$ point group, the dihedral angles are neither 0.00 nor 180.00 degree [15].

**Table 1. Geometrical structure for EMNQ2O as inhibitor in vacuum and in different solvents (DMSO and $H_2O$) as calculated by using DFT method.**

| Bond description | Bond length (Å) | Angle description | Angle (degree) | Dihedral angle description | Dihedral angle (degree) |
|---|---|---|---|---|---|
| **C1-C2** | 1.399 | **C2C1C10** | 120.076 | **C10C1C2C3** | 0.537 |
| **C1-C10** | 1.382 | **C2C1H** | 120.025 | **C10C1C2C12** | 179.606 |
| **C1-H** | 1.096 | **C1C2C3** | 119.522 | **C1C2C3C4** | -0.532 |
| **C2-C3** | 1.387 | **C1C2C12** | 119.532 | **C12C2C3C4** | -179.598 |
| **C2-C12** | 1.495 | **C2C3H** | 121.053 | **C2C3C4N** | -176.704 |
| **C3-C4** | 1.404 | **C3C4C9** | 119.719 | **C3C4N5N15** | 20.672 |
| **C4-C9** | 1.409 | **C3C4N5** | 120.390 | **C3C4N5C6** | 171.140 |
| **C4-N5** | 1.438 | **C4N5N15** | 115.756 | **N5N15C6O** | -17.717 |
| **N5-C6** | 1.451 | **N5C6C7** | 117.618 | **C4NC6C7** | 12.564 |
| **N5-N15** | 1.445 | **C7C6O14** | 124.619 | **OC6C7C8** | 174.005 |
| **C6-C7** | 1.466 | **C6C7C8** | 122.273 | **C6C7C8C9** | -0.465 |
| **C6-O14** | 1.221 | **C6C7H** | 116.185 | **C6C7C8C11** | -179.681 |
| **C7-C8** | 1.349 | **C7C8C9** | 120.277 | **C7C8C9C4** | 1.407 |
| **C8-C9** | 1.456 | **C7C8C11** | 119.964 | **C7C8C9C10** | -177.636 |
| **C8-C11** | 1.487 | **C9C10C1** | 121.320 | **C4C9C10C1** | -0.546 |
| **C9-C10** | 1.403 | **HC12H** | 105.679 | **C8C9C10C1** | -178.512 |
| **C12-H** | 1.108 | **C2C12H** | 110.436 | **NNC16C17** | 5.131 |
| **C12-C13** | 1.515 | **C12C13H** | 111.624 | **NNC16H** | -179.164 |
| **N15-C16** | 1.287 | **N5N15C16** | 122.631 | **NC16C17C** | -100.199 |
| **C18-N19** | 1.498 | **N15C16C17** | 128.803 | **C20C18N19O22** | -3.668. |
| **N19-O23** | 1.215 | **N15C16H** | 114.464 | **C21C18N19O23** | 176.456 |

Figure 2a shows the HOMO and LUMO density distributions for the optimized geometry of the studied inhibitor (in vacuum). The HOMO is mainly located on the (7-Ethyl-4-methyl-1-[(4-nitro-benzylidene)-amino]-1H-quinolin-2)-one moiety. This indicates that the preferred active-sites for an electrophilic attack are located within the region around the phenyl and nitrogen atoms. Moreover, the electronic density of LUMO is distributed at the aromatic ring and around the ring of (4-nitro-phenyl) moiety. Both HOMO and LUMO are located at the planar parts of the EMNQ2O molecule, Fig. 2b [15].

Baghdad Science Journal
P-ISSN: 2078-8665
E-ISSN: 2411-7986

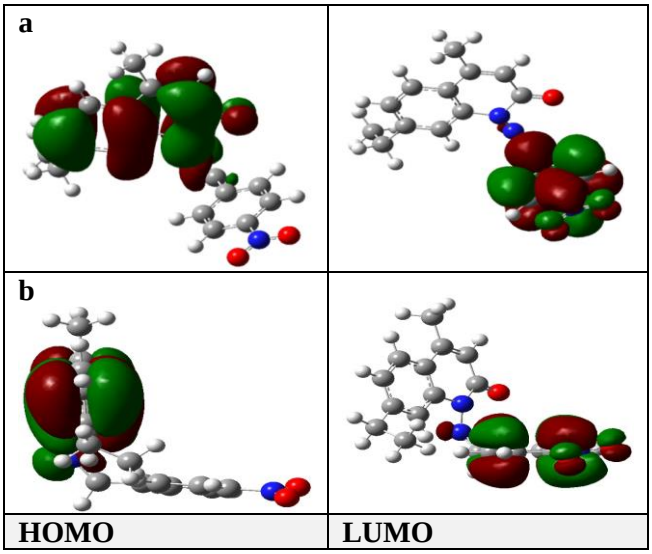


**Figure 2. a- Frontier molecular orbital density distributions of EMNQ2O compound.**
**b- the planar parts of the EMNQ2O molecule. [Red color: negatively charged lobe; green color: positive charge lobe].**

## Global molecular reactivity

Tables 2a and b show that EMNQ2O compound is a good inhibitor based on its values of the quantum corrosion efficiency parameters in the three media (vacuum and two polarity solvents). $E_{HOMO}$ (in vacuum) is -7.720 eV, be high in both DMSO and $H_2O$ solvents. $E_{LUMO}$ (in vacuum) is -2.964 eV which decreased in both solvents DMSO and $H_2O$. $\Delta E_{HOMO-LUMO}$ is 4.756 eV (in vacuum) and becomes less in both DMSO and $H_2O$ solvents. Dipole moment (μ in Debye) is a very important electronic parameter which results from the non-uniform distribution of charges on the various atoms in the molecule. The high value of dipole moment increases the adsorption between the inhibitor compound and the surface of the metal. Dipole moment for EMNQ2O inhibitor (in vacuum) is 6.4032 Debye, and becomes more in both DMSO as a result of increasing polarity of the solvent, meaning increasing inhibition efficiency.

The ionization potential, IP can be approximated as the negative of the highest occupied molecular orbital (HOMO) energy. Low values of IP increase the effectiveness of the inhibitor. The Ionization potential (IP) of the inhibitor in the vacuum is 7.720 eV, becomes less in DMSO and $H_2O$ solvents. The Electron-affinity (EA) is the amount of energy released when adding an electron to an atom or molecule. A high value of EA means less stable inhibitor (good corrosion inhibitor) [20]. The electron affinity of EMNQ2O in the vacuum is 2.964 eV, becomes more in DMSO or $H_2O$ solvents. Chemical hardness (η) is a measure of the ability of atom or molecule to transfer the charge. Increasing (η) decreases the stability of molecule, so the inhibitor possessed a low value of (η) which is considered to be a good inhibitor. The (η) value) in the vacuum is 3.835eV, becomes less in DMSO and $H_2O$ solvents.

Chemical softness (S) is a measure of the flexibility of an atom to receive electrons (S). Molecules having a high value of S are considered to be a good inhibitor. The values of S in the vacuum is 0.421 eV, becomes more in both DMSO and $H_2O$ solvents [10].

The electronegativity (**χ**) is the ability of an atom or a group to pull electrons, low electronegativity indicates a good inhibitor. The calculated (**χ**) in the vacuum is 5.342 eV, becomes less in both DMSO and $H_2O$ solvents.

Global electrophilicity index (**ω**) is the measure of the stability of an atom after gaining an electron. High value of (ω) meaning the molecule has a good inhibition. It was (6.000 eV) in the vacuum, becomes more in both DMSO and $H_2O$ solvents.

ΔN (difference in the number of electrons transferred). The fraction of electrons transferred (ΔN) from an inhibitor to carbon steel surface 0.348 of EMNQ2O has larger values in solvents compared with the vacuum, by the tendency of EMNQ2O molecule to receive the electrons from the metallic surface by Fe atoms in the unoccupied orbital of (3d). This ability increases the inhibition efficiency (IE) when two systems, Fe and inhibitor, are brought together. The net result of the order for inhibition efficiency is IE ($H_2O$)> IE (DMSO)> IE (Vacuum), meaning IE increase with increasing the polarity of the medium. From this, we conclude that the stability of the inhibitor is higher in both solvents than in vacuum. Equations [1-8] are used for calculating the chemical parameters [21-25]:

$$IP = -E_{HOMO} \quad (1)$$
$$EA = -E_{LUMO} \quad (2)$$
$$\Delta E = E_{LUMO} - E_{HOMO} \quad (3)$$
$$\eta = (IP - EA)/2 \quad (4)$$
$$\chi = (IP + EA)/2 \quad (5)$$
$$S = 1/\eta \quad (6)$$
$$\omega = \chi^2/2\eta \quad (7)$$
$$\Delta N = (\chi_{Fe} - \chi_{inhib})/[2(\eta_{Fe} + \eta_{inhib.})] \quad (8)$$

Whereas $\chi_{Fe}$ is 7.0 eV $mol^{-1}$; and $\eta_{Fe}$ is of 0.0 eV $mol^{-1}$ for carbon steel.

**Table 2. DFT calculations results for a- some physical properties and b- quantum chemical parameters for EMNQ2O inhibitor calculated at the optimized structure.**

| a<br>Inhibition Medium | Point group | Molecular formula | $E_{HOMO}$ (eV) | $E_{LUMO}$ (eV) | $\Delta E_{HOMO-LUMO}$ (eV) | μ (Debye) | $E_{total}$ (eV) |
|---|---|---|---|---|---|---|---|
| **Vacuum** | $C_1$ | | -7.720 | -2.964 | 4.756 | 6.4032 | -30597.352 |
| **DMSO** | $C_1$ | $C_{19}H_{17}N_3O_3$ | -6.342 | -3.259 | 3.083 | 7.6342 | -30596.859 |
| **Water** | $C_1$ | | -6.344 | -3.262 | 3.082 | 7.6660 | -30596.868 |

| b<br>Inhibition Medium | IP (eV) | EA (eV) | η (eV) | χ (eV) | S (eV) | ω (eV) | ΔN |
|---|---|---|---|---|---|---|---|
| **Vacuum** | 7.720 | 2.964 | 2.378 | 5.342 | 0.421 | 6.000 | 0.348 |
| **DMSO** | 6.342 | 3.259 | 1.542 | 4.800 | 0.648 | 7.470 | 0.713 |
| **Water** | 6.344 | 3.262 | 1.541 | 4.803 | 0.648 | 7.485 | 0.713 |

**Active sites of EMNQ2O inhibitor**

The inhibition of EMNQ2O inhibitor was done by using DFT Mulliken's charge population analysis in electron control unit (ecu), which gave an indication of the reactive centers of the molecules (electrophilic and nucleophilic sites). For that reason, the regions that have a large electronic charge are chemically softer than the regions that have a small electronic charge. Thus, the density of electron plays an important role in the chemical reactivity calculating. The chemical adsorption interactions are either by orbital interactions or electrostatic. The sites of nucleophilic attack will be the place where the positive charge value is a maximum, thus only the charges on the oxygen (O), nitrogen (N), and some carbon atoms are presented. In turn, the site of electrophilic attack was controlled by the negative charge value. The nucleophilic and electrophilic electronic charge values of compounds in DMSO and $H_2O$ solutions are higher than in vacuum. Table 3 shows the order of the nucleophihic reactive sites of EMNQ2O inhibitor as follows: C4 > C11 > C18 > C16 > C14 > C3; whereas the order of the electrophilic reactive sites is: C2 > C17 > C8 > C9 > C5.

**Table 3. Mulliken charge population analysis for EMNQ2O molecule calculated in three media (vacuum, DMSO, and $H_2O$) by DFT method.**

| Atom | Electronic Charge (ecu) | Atom | Electronic charge (ecu) | Atom | Electronic Charge (ecu) | Atom | Electronic Charge(ecu) |
|---|---|---|---|---|---|---|---|
| | -0.878V | | -0.054V | | -0.489V | | -0.010V |
| **C1** | -0.127D | **C7** | -0.270D | **C13** | -0.645D | **N19** | -0.137D |
| | -0.126H | | -0.271H | | -0.646H | | -0.136H |
| | 0.862V | | 0.602V | | -0.470V | | -0.162V |
| **C2** | 0.937D | **C8** | 0.651D | **O14** | -0.407D | **C20** | -0.059D |
| | 0.936H | | 0.651H | | -0.409H | | -0.059H |
| | -0.354V | | 0.434V | | -0.058V | | -0.184V |
| **C3** | -0.408D | **C9** | 0.581D | **N15** | -0.225D | **C21** | -0.159D |
| | -0.408H | | 0.581H | | -0.226H | | -0.158H |
| | -0.399V | | -0.372V | | -0.129V | | -0.139V |
| **C4** | -0.691D | **C10** | -0.488D | **C16** | -0.480D | **O22** | -0.049D |
| | -0.690H | | -0.488H | | -0.481H | | -0.050H |
| | 0.019V | | -0.324V | | 0.324V | | -0.132V |
| **N5** | 0.570D | **C11** | -0.523D | **C17** | 0.802D | **O23** | -0.048D |
| | 0.570H | | -0.524H | | 0.804H | | -0.050H |
| | 0.008V | | -0.149V | | 0.115V | | |
| **C6** | -0.113D | **C12** | -0.200D | **C18** | -0.482D | | |
| | -0.112H | | -0.200H | | -0.482H | | |

V: vacuum; D: dimethyl sulfoxide; H: water; ecu: electron control unit.

**Corrosion inhibition measurement**

**Potentiodynamic polarization measurements**

The parameters of the electrochemical corrosion are listed in Table 4 such as corrosion potential ($E_{corr}$), Tafel slopes (bc and/or ba) and corrosion current density ($I_{corr}$) obtained by cathodic and anodic regions of Tafel lines. Figs. 3 and 4 present potentiodynamic polarization curves for C.S in salt and acid solutions containing different concentrations of EMNQ2O compound. IE%, Θ, can be measured using equations [8-11].

$$\%IE = \frac{i_{corr(un)} - i_{corr(in)}}{i_{corr(un)}} \times 100 \ldots . (8)$$

Where $i_{corr\ (in)}$ is the inhibited corrosion current densities; $i_{corr\ (un)}$ is the uninhibited current densities. The values of polarization resistance (Rp) can be calculated using equation 9.

$$Rp = \frac{b_a \times b_c}{2.303(b_a + b_c) \times i_{corr}} \quad (9)$$

The surface coverage ( Θ ) of the carbon steel corrosion immersed in 3.5% NaCl and acidic solutions containing different EMNQ2O concentrations (C) can be estimated using equation 10.

$$\Theta = \frac{\%IE}{100} \quad (10)$$

The corrosion rate (CR) can be calculated using equation 11:

$$CR = i_{corr} \times 0.249 \ldots \quad (11)$$

The addition of the quinolin-2-one derivative leads to a decrease in the corrosion rate i.e the conversion of cathode and anode curves to lower values of the current density. Both cathode and anode corrosion reactions in C.S (carbon 45) electrode were prevented by EMNQ2O in both 3.5% NaCl and 0.5M HCl solution. Figs. 3 and 4 show Tafel lines of anodic and cathodic polarization curves for the corrosion of carbon steel in the salty and in the acidic solution respectively, with and without the addition of various concentrations of EMNQ2O inhibitor as well as the optimum conditions of (20ppm) inhibitor and (at 293K) temperature.

Tables 4 and 5 list the corrosion rate values of C.S and inhibition efficiencies of various inhibitor concentrations measured at salty and acidic solutions at different temperature, respectively. The tables show that increasing temperature leads to increasing the corrosion current densities $I_{corr.}$. While the efficiencies IE% is enhanced with the increasing of the inhibitor concentration. The optimum conditions for EMNQ2O in the salty and in the acidic solutions were found at 293K temperature and 20ppm inhibition concentration both corresponded to the lowest $I_{corr}$ of 37.84 ($\mu A.cm^{-2}$) and the maximum IE% of 94.98 (%) in the salty solution and lowest $I_{corr.}$ of 6.68 ($\mu A.cm^{-2}$) and the maximum IE% of 80.75 (%) in the acidic solution, respectively. The values of iron corrosion rate CR decreased with the increase of EMNQ2O concentration. The addition of the inhibitor to the blank solution increases the cathodic and anodic current densities without shifting the corrosion potential. The EMNQ2O inhibitor therefore can be described as a mixed-type inhibitor in which its inhibition action is caused by the adsorption process. The inhibition action is a proportional of the reduction reaction area on the carbon steel surface [15].

**Table 4. Electrochemical data of C.S corrosion in salty solution at different concentrations of EMNQ2O compound.**

| Inhib. conc. | T (K) | $E_{corr}$ (mV) | $i_{corr}$ ($\mu A.cm^{-2}$) | Bc ($mV.dec^{-1}$) | ba ($mV.dec^{-1}$) | IE% | Θ | CR |
|---|---|---|---|---|---|---|---|---|
| | 293 | -408.0 | 133.13 | -230.4 | 138.5 | ------ | ------ | 33.15 |
| **Blank** | 303 | -446.7 | 172.04 | -279.6 | 110.2 | ------ | ------ | 42.84 |
| **0ppm** | 313 | -491.2 | 189.34 | -269.0 | 96.5 | ------ | ------ | 47.15 |
| | 323 | -547.7 | 192.99 | -252.9 | 84.4 | ------ | ------ | 48.05 |
| | 293 | -461.2 | 18.05 | -136.6 | 56.3 | 86.44 | 0.864 | 4.49 |
| **5ppm** | 303 | -459.9 | 25.94 | -195.4 | 58.9 | 84.92 | 0.849 | 6.46 |
| | 313 | -441.0 | 34.30 | -104.9 | 76.9 | 81.88 | 0.819 | 8.54 |
| | 323 | -521.2 | 43.23 | -232.6 | 83.5 | 77.59 | 0.776 | 10.76 |
| | 293 | -411.5 | 17.13 | -43.6 | 35.8 | 87.13 | 0.871 | 4.27 |
| **10ppm** | 303 | -460.4 | 23.53 | -62.6 | 44.5 | 86.32 | 0.863 | 5.86 |
| | 313 | -472.2 | 31.04 | -96.2 | 57.7 | 83.60 | 0.836 | 7.73 |
| | 323 | -490.1 | 42.41 | -180.4 | 63.9 | 78.02 | 0.780 | 10.56 |
| | 293 | -359.8 | 6.68 | -43.3 | 38.7 | 94.98 | 0.950 | 1.66 |
| **20ppm** | 303 | -407.4 | 24.83 | -74.5 | 50.2 | 85.56 | 0.856 | 6.18 |
| | 313 | -378.6 | 32.03 | -93.9 | 60.2 | 83.08 | 0.830 | 7.98 |
| | 323 | -552.8 | 38.29 | -278.5 | 89.6 | 80.15 | 0.801 | 9.53 |

Baghdad Science Journal
2022, 19(1): 105-120
P-ISSN: 2078-8665
E-ISSN: 2411-7986

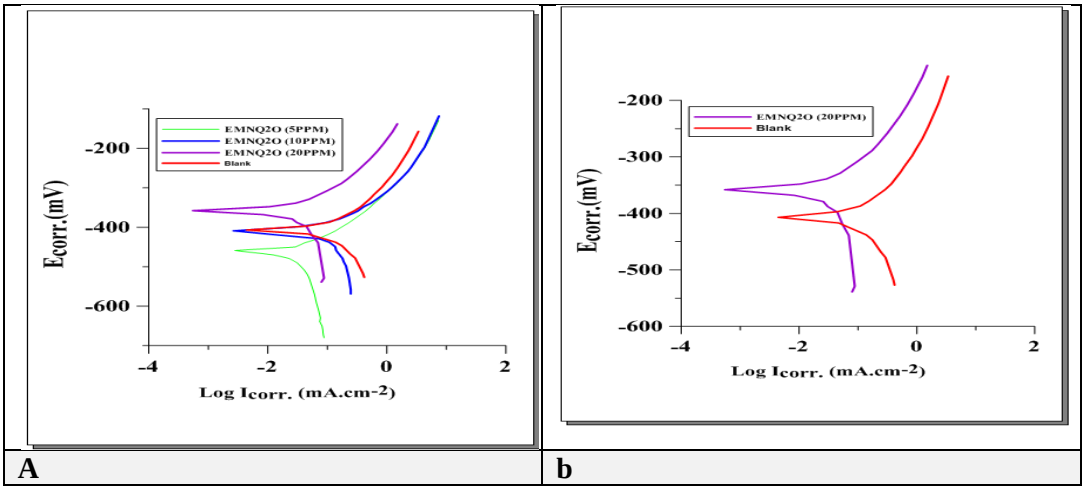


**Figure 3. Polarisation curve of carbon steel in seawater at 293 (K) for EMNQ2O compound; (a) at different concentrations, and (b) at the optimum concentration.**

**Table 5. Electrochemical data of carbon steel corrosion in acid solution at different concentrations for EMNQ2O compound.**

| Inhib. conc. | T (K) | $E_{corr}$ (mV) | $i_{corr}$ ($\mu A.cm^{-2}$) | Bc ($mV.dec^{-1}$) | ba ($mV.dec^{-1}$) | IE% | Ɵ | CR |
|---|---|---|---|---|---|---|---|---|
| **Blank 0ppm** | 293 | -340.2 | 196.59 | -132.9 | 76.1 | ------ | ------ | 48.95 |
| | 303 | -349.9 | 285.76 | -129.4 | 87.4 | ------ | ------ | 71.15 |
| | 313 | -336.8 | 383.29 | -123.8 | 77.4 | ------ | ------ | 95.44 |
| | 323 | -326.9 | 495.50 | -107.5 | 58.6 | ------ | ------ | 123.38 |
| **5ppm** | 293 | -412.2 | 56.59 | -61.1 | 49.6 | 72.00 | 0.720 | 14.09 |
| | 303 | -413.7 | 89.19 | -58.8 | 45.8 | 71.21 | 0.712 | 22.21 |
| | 313 | -413.6 | 107.32 | -47.7 | 45.2 | 68.78 | 0.688 | 26.72 |
| | 323 | -411.7 | 196.02 | -50.6 | 46.8 | 60.43 | 0.604 | 48.81 |
| **10ppm** | 293 | -402.2 | 41.45 | -46.4 | 44.0 | 78.91 | 0.789 | 10.32 |
| | 303 | -399.3 | 74.73 | -62.4 | 51.2 | 73.84 | 0.738 | 18.61 |
| | 313 | -410.2 | 107.92 | -49.9 | 53.1 | 71.84 | 0.718 | 26.87 |
| | 323 | -401.3 | 160.74 | -50.2 | 45.9 | 67.56 | 0.676 | 40.02 |
| **20ppm** | 293 | -410.9 | 37.84 | -59.7 | 42.4 | **81.40** | 0.814 | 9.42 |
| | 303 | -405.0 | 53.14 | -63.6 | 52.5 | 80.75 | 0.808 | 13.23 |
| | 313 | -405.0 | 96.09 | -81.5 | 63.7 | 75.20 | 0.752 | 23.93 |
| | 323 | -404.6 | 122.84 | -54.1 | 55.6 | 74.93 | 0.749 | 30.59 |

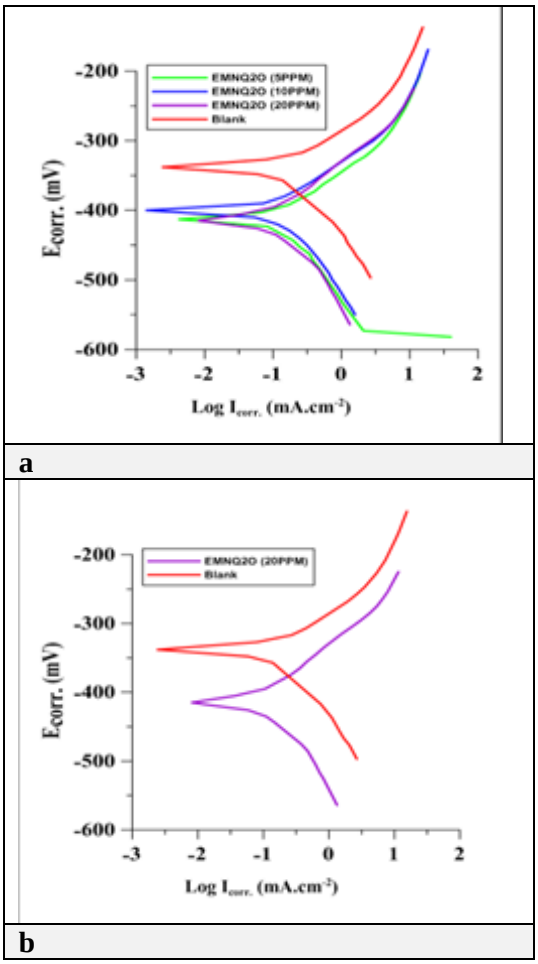


**Figure 4. Polarisation curve of carbon steel in acidic solution at 293 (K) for EMNQ2O compound; (a) at different concentrations, and (b) at the optimum concentration.**

**Corrosion kinetic and thermodynamic activation parameters**

Arrhenius law is presented as a straight line of the logarithm of the corrosion rate. The activation parameters were calculated with and without inhibitors at different concentrations. The activation energy of the corrosion process ($E_a$), and the pre-exponential factor (A), were calculating from the slope and intercept of plotting log ($I_{corr}$) against (1/ T) equation 12, Figs. 5 and 7 for salty and acidic media, respectively. All $E_a$ values in presence of EMNQ2O inhibitor are higher than that of the blank (09.6348 kJ/ mol) for the salty solution and (24.1828 kJ/ mol) for the acidic solution which means that the corrosion reaction of C.S is retarded by EMNQ2O inhibitor. These observations support the physical observation. Plot of log (CR/ T) or log ($I_{corr}$/ T) against (1/ T), gave a linear relationship with the slope of (−ΔH*/ 2.303R) and intercept of [log(R/ Nh)+ (ΔS*/ 2.303R)] equation (13), as shown in Figs. 6 and 8 for salty and acidic media, respectively.

$$\text{Log } (I_{corr}) = \text{Log } A - E_a / 2.303RT \quad (12)$$

$$\text{Log } (I_{corr}/ T)) = \log (CR/ T) = \text{Log } (R/ N h) + \Delta S^*/ 2.303R - \Delta H^*/ 2.303RT \quad (13)$$

Where ($I_{corr}$) is the corrosion current density which is equal to the corrosion rate (CR), (R) is the universal gas constant (8.314 J $mol^{-1}$ $K^{-1}$), (T) is the absolute temperature in K, (h) is Planck's constant (6.626 x $10^{-34}$ J s), (N) is Avogadro's number (6.022 x $10^{23}$ $mol^{-1}$), ΔH* is the enthalpy of activation and (ΔS*) is the entropy of activation.

Accordingly, the activation thermodynamic parameters (ΔH* and ΔS*) were calculated in salty and acidic media, respectively, as shown in Tables 6 and 7. Positive values of (ΔH*) for the corrosion reaction in 3.5% NaCl and in acidic media at the temperature range of (293-323) K and different concentrations support the endothermic nature of this reaction [16]. Whereas negative values of (ΔS*) for the corrosion reaction reveals that an increase in disordering takes place on going from reactant to the activated complex [17]. The values of ΔH*, ΔS* and Ea* obtained in presence of EMNQ2O inhibitor are higher than those obtained in the blank solution. This observation further supports the proposed physical mechanism. The values of ΔG* for corrosion reaction were calculated from equation 14. The positive values of ΔG* indicating that the transition state of the adsorption process is not spontaneous.

$$\Delta G^* = \Delta H^* - T\Delta S^* \quad (14)$$

**Table 6. Corrosion kinetic parameters for carbon steel in 3.5% NaCl solution for blank and with various concentrations of EMNQ2O inhibitor.**

| Conc. (ppm) | ΔG* (kJ/ mol) | | | | ΔH* kJ/ mol | ΔS* kJ/ mol K | $E_a$* kJ/ mol | A Molecule/ $cm^2$ S |
|---|---|---|---|---|---|---|---|---|
| | 293K | 303K | 313K | 323K | | | | |
| Blank 0 | 63.072 | 64.983 | 66.894 | 68.805 | 7.080 | -0.1911 | 09.6360 | 1.10E+27 |
| 5 | 68.015 | 69.643 | 71.271 | 72.899 | 20.315 | -0.1628 | 22.8713 | 3.31E+28 |
| 10 | 68.187 | 69.797 | 71.407 | 73.017 | 21.014 | -0.1610 | 23.5701 | 4.07E+28 |
| 20 | 66.320 | 77.562 | 68.804 | 70.046 | 29.929 | -0.1242 | 43.7838 | 8.65E+31 |

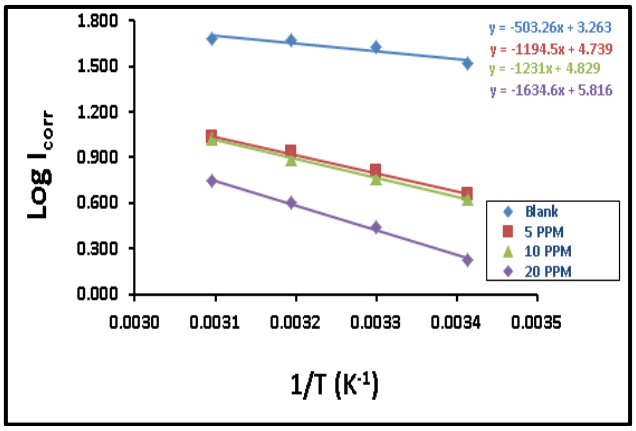


**Figure 5. Plotting log ($I_{corr}$) against (1/ T) for carbon steel in salty solution in absence (blank) and in presence of different concentrations of the EMNQ2O inhibitor.**

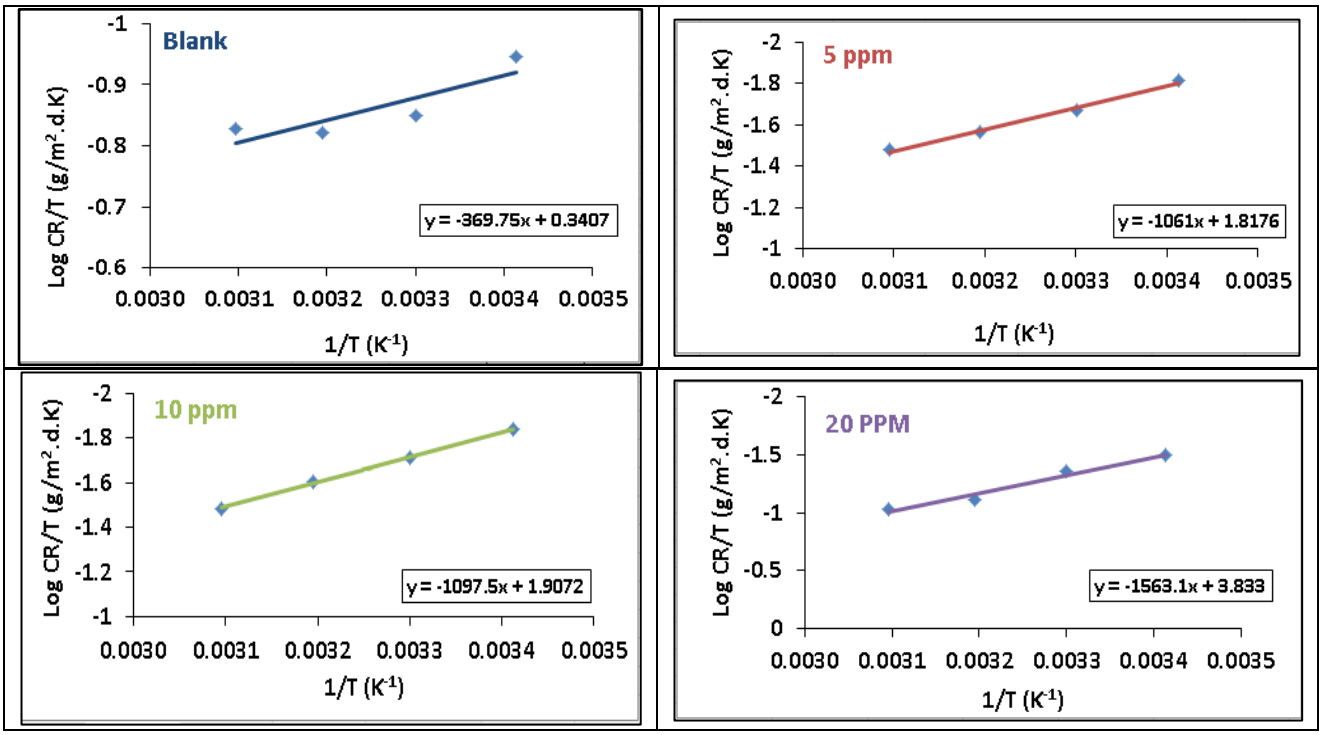


**Figure 6. Plotting log (CR/ T) against (1/ T) of carbon steel in salty solution for in absence (blank) and in presence of different concentrations of the EMNQ2O inhibitor.**

**Table 7. Corrosion kinetic parameters for carbon steel in acid medium for blank and with various concentrations of the inhibitor.**

| Conc. (ppm) | ΔG* (kJ/ mol) | | | | ΔH* kJ/ mol | ΔS* kJ/ mol K | Ea kJ/ mol | A Molecule/ $cm^2$ S |
|---|---|---|---|---|---|---|---|---|
| | 293K | 303K | 313K | 323K | | | | |
| Blank 0 | 57.869 | 59.106 | 60.343 | 61.580 | 21.625 | -0.1237 | 24.1828 | 6.15E+29 |
| 5 | 65.323 | 66.592 | 67.861 | 69.130 | 28.141 | -0.1269 | 30.6967 | 2.48E+30 |
| 10 | 65.929 | 67.073 | 68.217 | 69.361 | 32.410 | -0.1144 | 32.4870 | 3.43E+30 |
| 20 | 66.320 | 67.562 | 68.804 | 70.046 | 29.929 | -0.1242 | 34.9665 | 1.11E+31 |

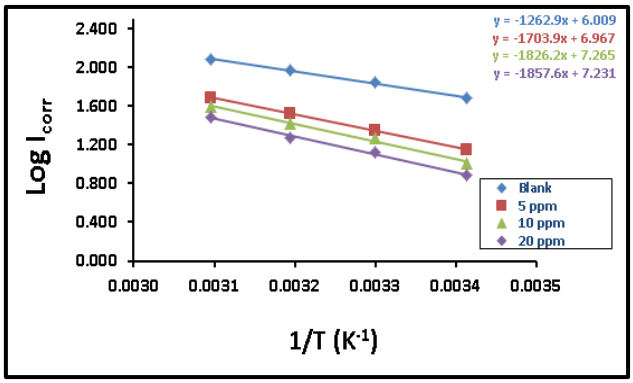


**Figure 7. Plotting log ($I_{corr}$) against (1/ T) for carbon steel in acidic solution in absence (blank) and in presence of different concentrations of the EMNQ2O inhibitor.**

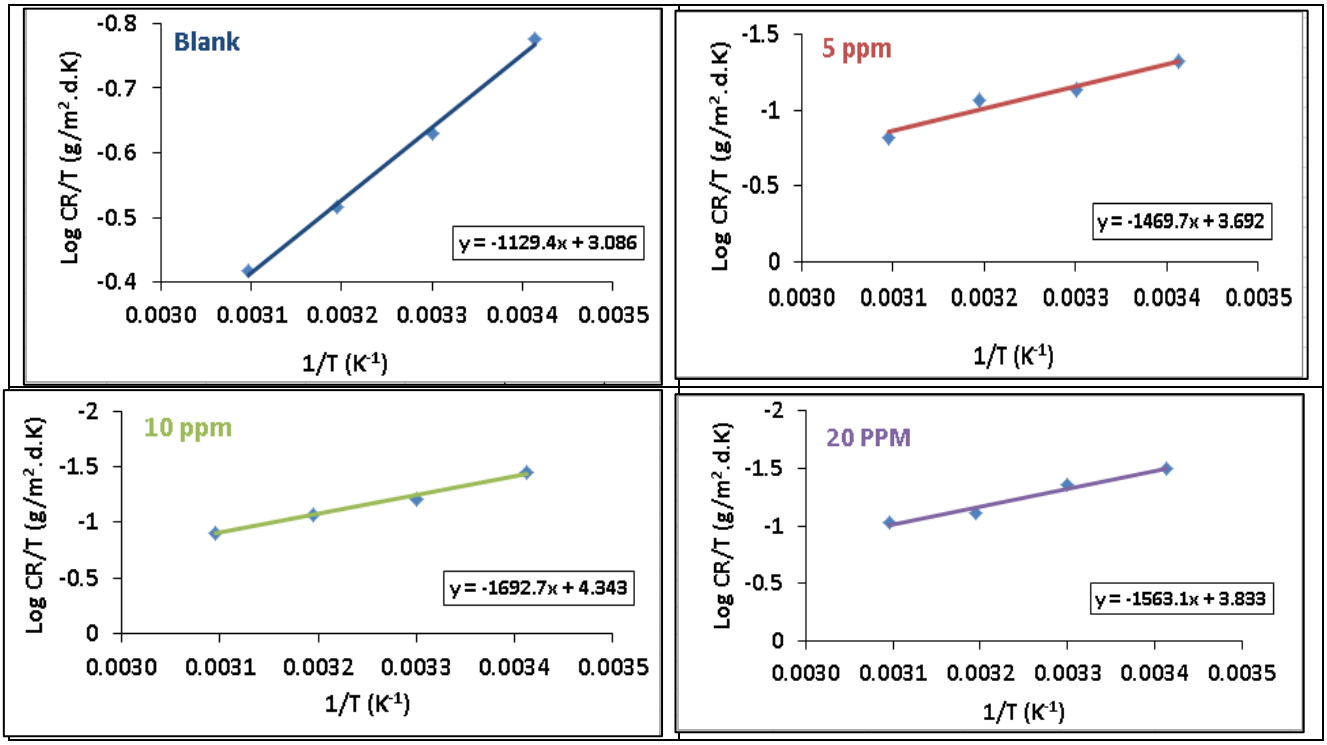


**Figure 8. Plotting log (CR/ T) against (1/ T) of carbon steel in acidic solution in absence (blank) and in presence of different concentrations of the EMNQ2O inhibitor.**

**Adsorption isotherm**

The adsorption isotherms are essential in characterizing the reaction between carbon steel surface and inhibitor molecules. Langmuir adsorption isotherm is the most frequently used isotherms. It can be described by the following equation:

$$C/\Theta = (1/K_{ads}) + C \quad (15)$$

Whereas C is the inhibitor concentration in 3.5% NaCl and 0.5M HCl, $K_{ads}$ is the adsorption equilibrium constant and Θ is the surface coverage. The dependence of the (C/ Θ) fraction as a function of (C) for EMNQ2O in salty and acidic solutions is shown in Figs. 9 and 11. It can be used to determine $K_{ads}$. The adsorption equilibrium constant has a relation with the free energy of adsorption ($\Delta G_{ads}$) through the following equation [15]:

$$K_{ads} = (1/55.55) \exp(\Delta G_{ads}/ RT) \quad (16)$$

Here R is the gas constant (J $K^{-1}$ $mol^{-1}$), T is the absolute temperature (K) and 55.5 is the molar concentration of water in the solution (mol $L^{-1}$), So the values of $\Delta G_{ads}$ at different temperature were obtained from equation 17. Enthalpy value of adsorption ($\Delta H°_{ads}$) was obtained from the slope of Vant Hoff equation expressed by equation 18, and entropy value of adsorption ($\Delta S°_{ads}$) was obtained from the intercept of the same equation (Figs. 10 and 12).

$$\Delta G°_{ads} = -2.303RT \log K_{ads} \quad (17)$$

$$\Delta G°_{ads} = \Delta H°_{ads} - T\Delta S°_{ads}$$

$$\log K_{ads} = -\Delta H°_{ads}/ 2.303RT + \Delta S°_{ads}/ 2.303R \quad (18$$

Tables 8 and 9 list the thermodynamic functions of EMNQ2O inhibitor on C.S surface in 3.5% NaCl and 0.5M HCl at various temperatures, respectively. Higher values of $K_{ads}$ obtained from Langmuir isotherm for EMNQ2O indicate strong adsorption on the carbon steel in 3.5% NaCl and 0.5M HCl. Negative values of $\Delta G°_{ads}$ indicate spontaneous adsorption process. The values of $\Delta G°_{ads}$ around -20 (kJ/mol) or less negative consisted with the electrostatic interaction (physic-sorption); while those values of -40 (kJ/mol) or more negative involve electron transfer which leads to form a chemical bond (chemisorptions) [26].

The calculated values for $\Delta G°_{ads}$ were found in the range of -49.652 to -40.929 (kJ $mol^{-1}$) at different temperatures (293-323K) in the salty medium, while, $\Delta G°_{ads}$ were found in the range of -39.394 to -40.612 (kJ $mol^{-1}$) at different temperatures (293-323K) in the acidic medium. These values indicate that the adsorption of EMNQ2O follows physisorption processing. The obtained entropy $\Delta S°_{ads}$ value is positive which confirms that the corrosion process is entropically favorable [19]. The negative value of $\Delta H°_{ads}$ in the salt and acidic media indicates an exothermic process for the adsorption of inhibitory molecules on the C.S surface. For EMNQ2O compound, $\Delta H°_{ads}$ is equal to -89.442 (kJ $mol^{-1}$) in the salt medium, and equal to -24.537 (kJ $mol^{-1}$) in acidic medium (Tables 8 and 9**)**.

**Table 8. Thermodynamic parameters for adsorption of (EMNQ2O) compound on C.S surface in 3.5% NaCl at various temperatures.**

| T K | $K_{ads}$ L $mol^{-1}$ | $\Delta G°_{ads}$ kJ. $mol^{-1}$ | $\Delta H°_{ads}$ kJ.$mol^{-1}$ | $\Delta S°_{ads}$ kJ.$mol^{-1}$ |
|---|---|---|---|---|
| 293 | $2.6*10^5$ | -41.480 | -89.442 | 0.438 |
| 303 | $3.3*10^5$ | -40.929 | | |
| 313 | $8.8*10^5$ | -43.953 | | |
| 323 | $9.0*10^5$ | -49.652 | | |

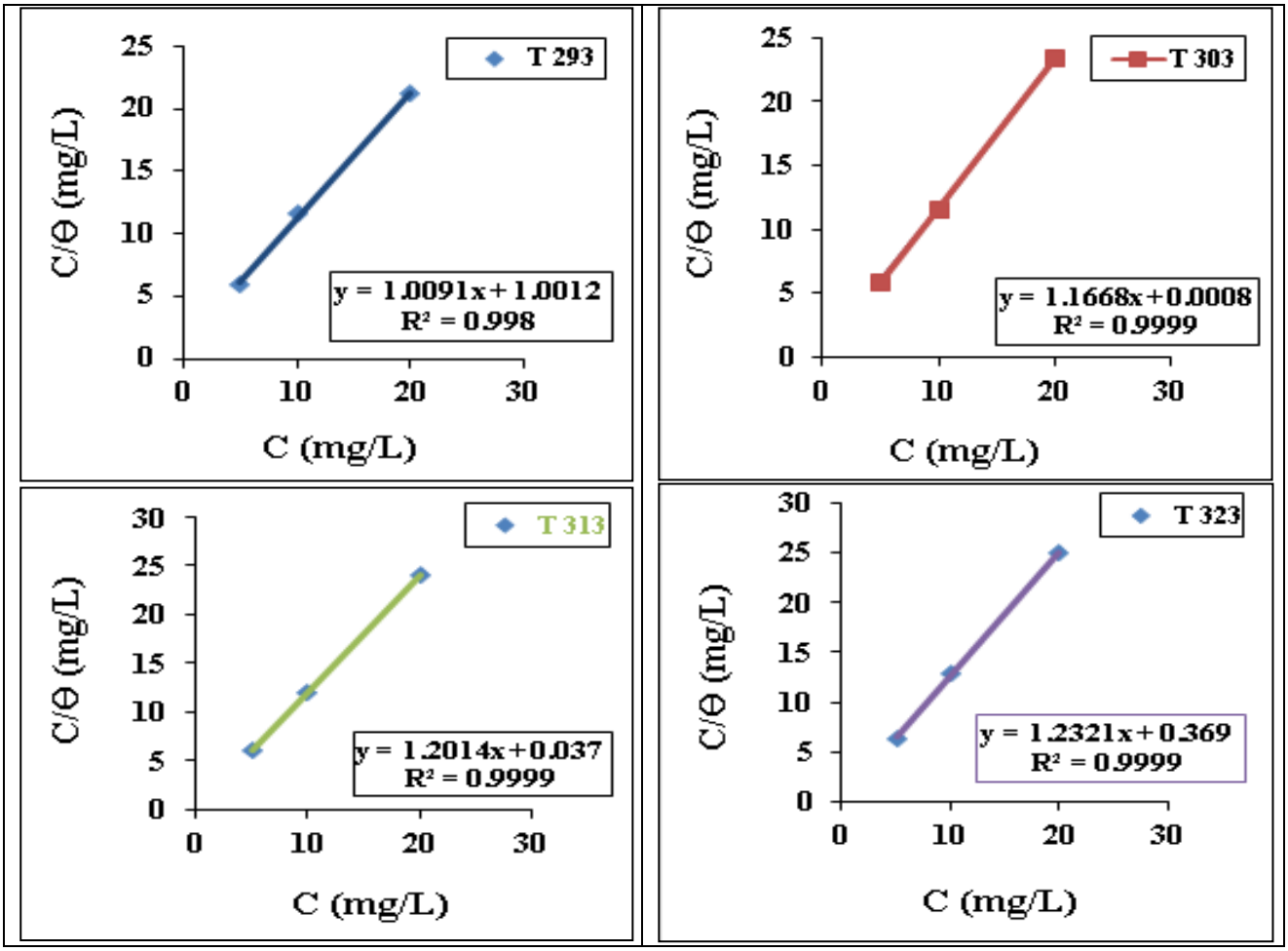


**Figure 9. Langmuir isotherms plot for the adsorption EMNQ2O inhibitor on carbon steel in salty medium at temperatures of (293, 303, 313 and 323) K.**

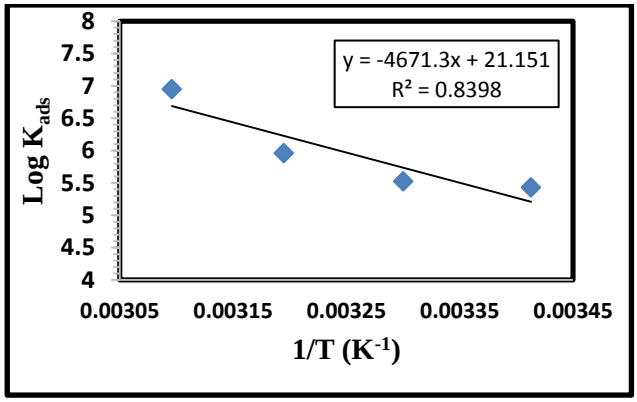


**Figure 10. Plotting of log $K_{ads}$ against (1/ T) for EMNQ2O compound.**

**Table 9. Langmuir parameters for adsorption of (EMNQ2O) compound on carbon steel surface in 0.5M HCl solution at different temperatures.**

| T K | $K_{ads}$ L $mol^{-1}$ | $\Delta G°_{ads}$ kJ. $mol^{-1}$ | $\Delta H°_{ads}$ $kJ.mol^{-1}$ | $\Delta S°_{ads}$ $kJ.mol^{-1}$ |
|---|---|---|---|---|
| 293 | $1.4*10^5$ | -41.492 | -24.537 | 0.216 |
| 303 | $1.9*10^5$ | -40.612 | | |
| 313 | $3.4*10^5$ | -41.654 | | |
| 323 | $6.0*10^5$ | -39.394 | | |

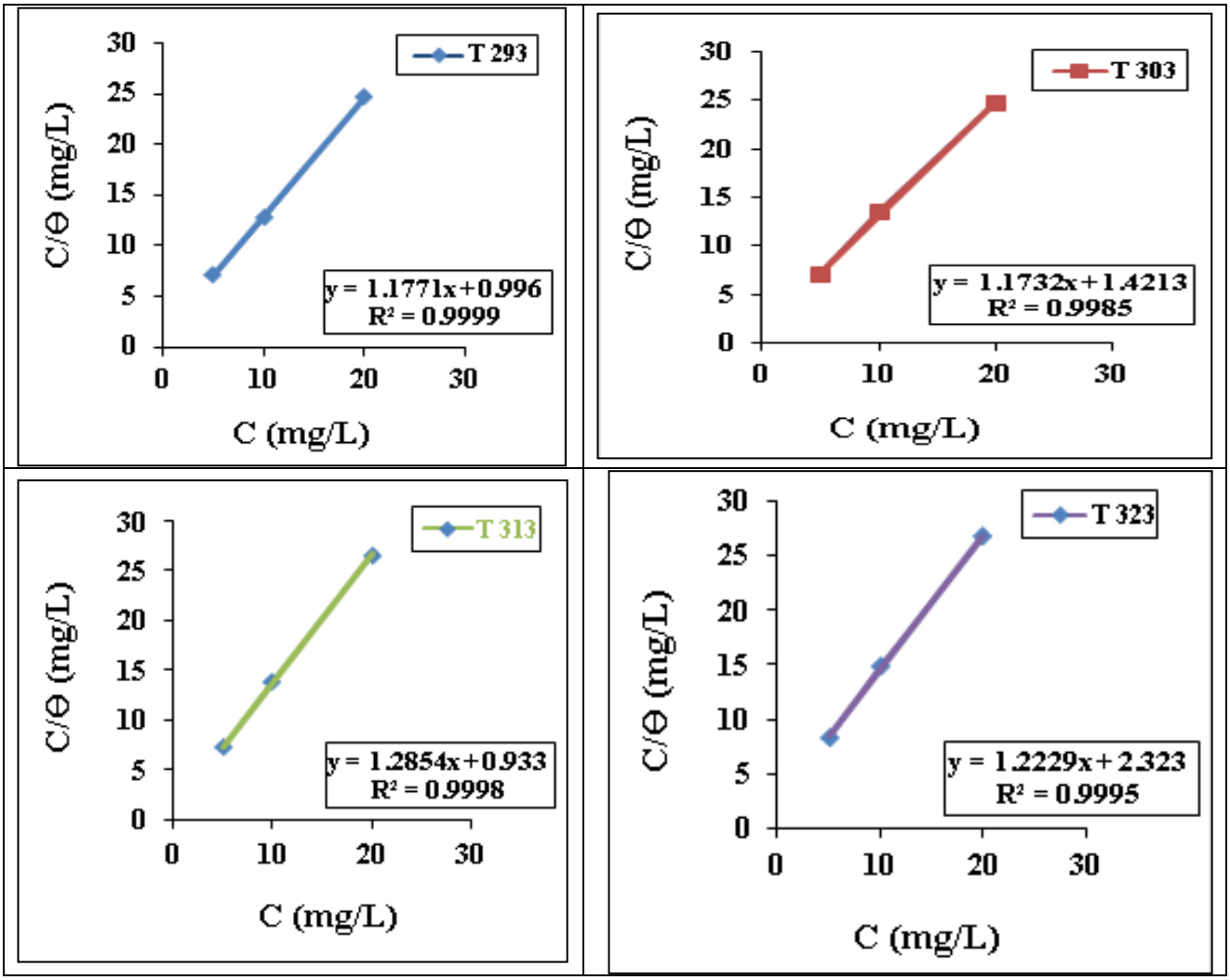


**Figure 11. Langmuir isotherms plot for the adsorption of EMNQ2O inhibitor on carbon steel in acidic medium at temperatures of (293, 303, 313 and 323) K.**

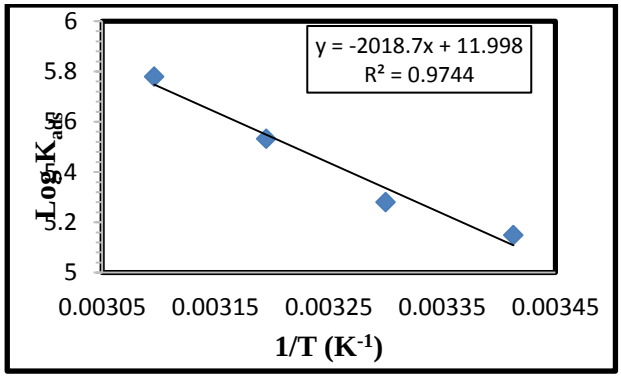


**Figure 12. Plotting log $K_{ads}$ against (1/ T) for EMNQ2O compound in acid solution.**

**Scanning Electron Microscopy (SEM):**

The SEM micrographs of the corroded carbon steel in 3.5% NaCl and 0.5M HCl solutions in the prescience and absence of EMNQ2O inhibitor are shown in Figs. 13 and 14, respectively. In images (a) of these figures (absence of inhibitor of carbon steel surface), a clear damage is obvious on the metal surface. In contrast, Figs. 13b and 14b show a remarkable improvement in the metal surface morphology due to the presence of EMNQ2O inhibitor which is responsible for forming a protective film of an insoluble complex on carbon steel surface ($Fe^{2+}$-EMNQ2O complex).

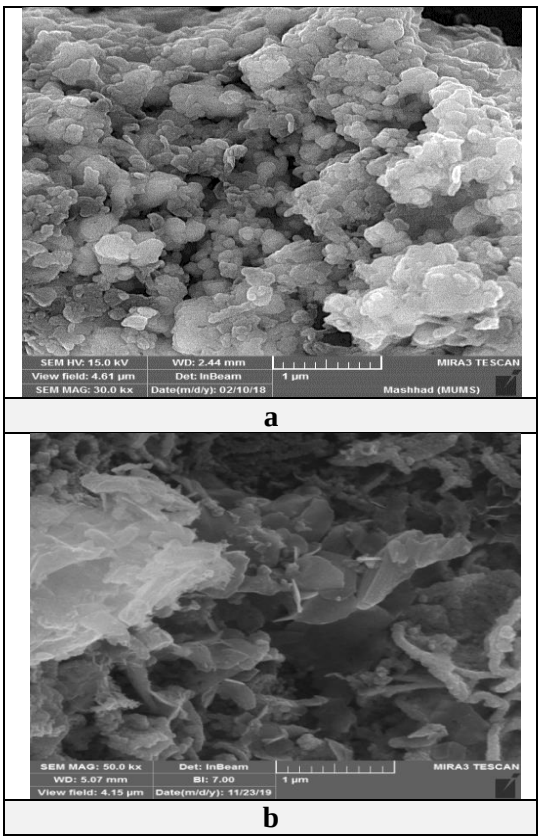


**Figure 13. SEM of C.S surface (a) in salt medium of 3.5% NaCl solution without presence of EMNQ2O inhibitor, (b) in presence of 20 ppm of EMNQ2O inhibitor.**

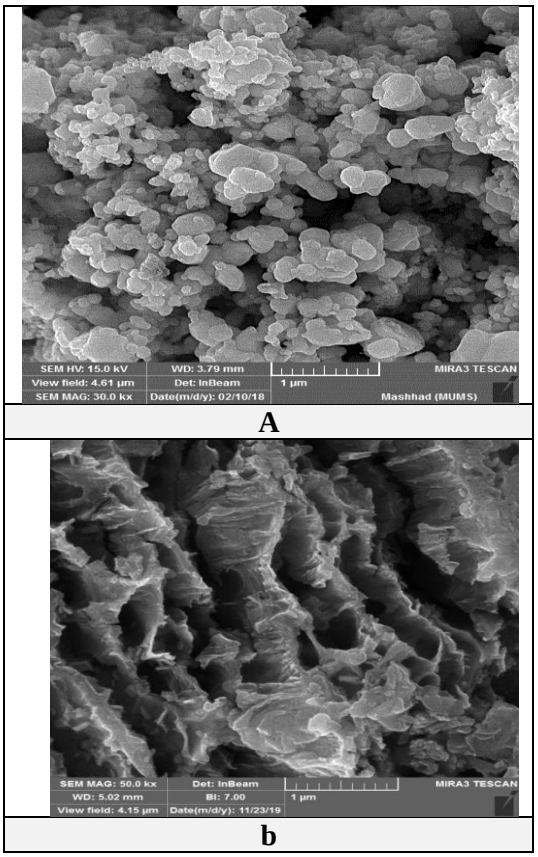


**Figure 14. SEM of C.S surface (a) in acidic solution without presence of EMNQ2O inhibitor, (b) in presence of 20 ppm of EMNQ2O inhibitor.**

**Atomic force microscopy characterization**

AFM is a technique for obtaining the surface morphology at (Nano to micro-scale) and has become a good choice for studying the influence of inhibitor on the generation and the progress of the corrosion at the metal interface. AFM image analysis was performed to obtain the average roughness (Ra), the root-mean-square roughness (Rq), and the maximum peak–to–valley (P-V) height values. Figures 15a, 16a show the corroded metal surface in the absence of the inhibitor immersed in 3.5% NaCl and 0.5M HCl solution, respectively. In this case, the Rq, Ra and P-V height values for the carbon steel surface observed are (28.2nm, 34.1nm, and 184nm) in 3.5% NaCl solution, and (17.24nm, 21.45nm, and 127.89nm) in 0.5M HCl solution. In the presence of 20ppm of EMNQ2O inhibitor, they are less and had been (154nm, 17nm, and 63.9nm) in salt environment and (9.1nm, 10.7nm, and 39.8nm) in the acidic environment. These parameters confirm that the surface is smoother, (Figs. 15b, 16b). Surface smoothness results from the formation of a compact ($Fe^{2+}$-EMNQ2O complex) protective layer on the metal surface, thus preventing corrosion of carbon steel. These data indicate that the surface of carbon steel immersed in the saline and acidic

Baghdad Science Journal
P-ISSN: 2078-8665
E-ISSN: 2411-7986

solution has a greater surface roughness in the blank than in the presence of the inhibitor, which indicates that the surface of the unprotected soft steel is harder due to the corrosion of carbon steel in salt and acid environments [27-30].

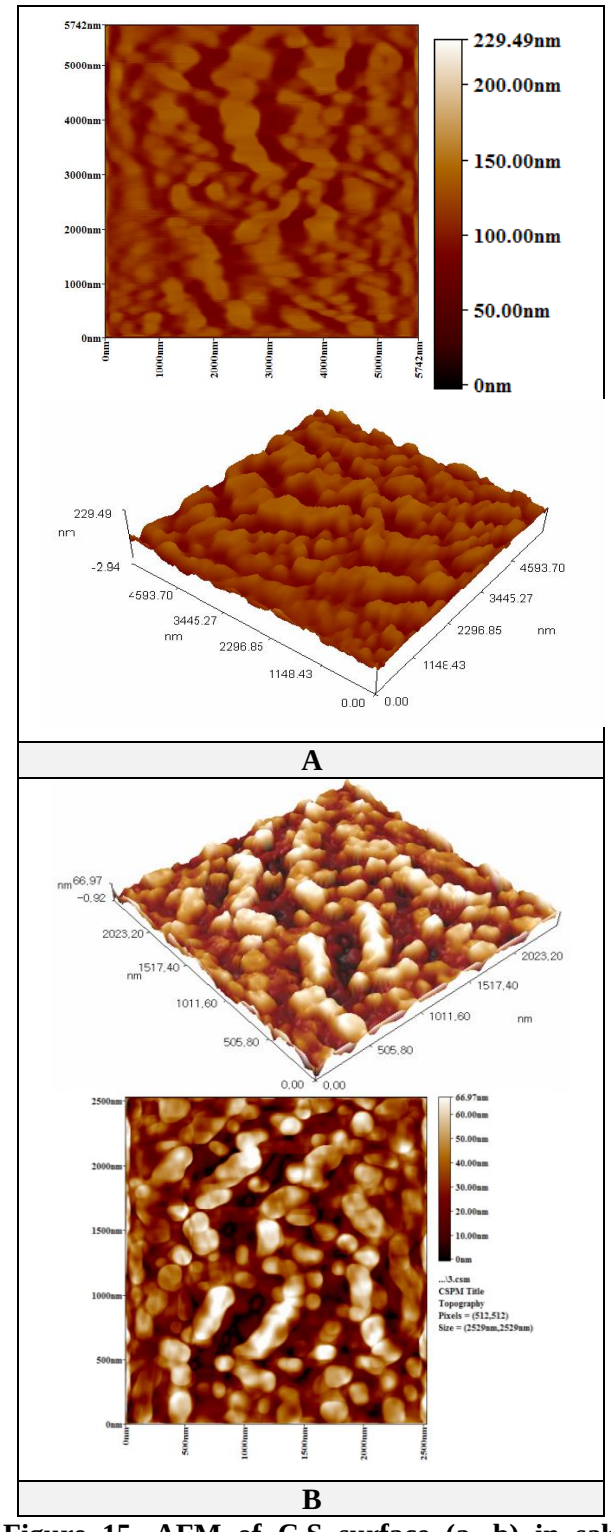


**Figure 15. AFM of C.S surface (a, b) in salt medium of 3.5% NaCl solution without presence of the (EMNQ2O) inhibitor, (c, d) in presence of 20 ppm of (EMNQ2O) inhibitor.**

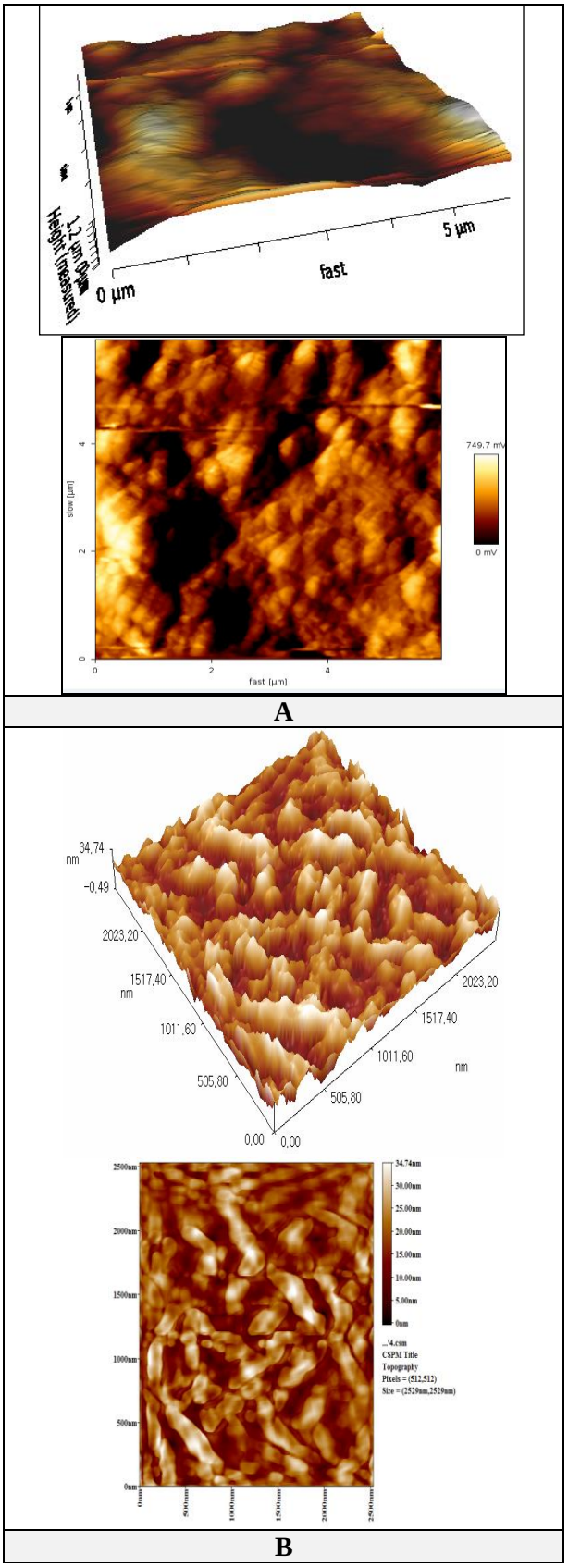


**Figure 16. AFM of C.S surface (a, b) in acidic solution without presence of the (EMNQ2O) inhibitor, (c ,d) in presence of 20 ppm of (EMNQ2O) inhibitor.**

## Conclusions:

- The results of DFT calculations on EMNQ2O quinoline derivative have been presented in vacuum, DMSO and in water solutions. The HOMO, LUMO, and charges on atoms predict a similar center that would prefer to be attacked by nucleophilic or electrophilic species.
- The ΔE and dipole moment values suggest that EMNQ2O has greater tendency to interact with the metal surface in solvent solutions than in vacuum, and it is a good inhibitor in both of them.
- Quantum chemical calculations of (DFT/ B3LYP/ 6-311++G/ 2d, 2p) gave realistic results in the case of the geometry of the conformers, and the results of DFT/B3LYP were closer to the experimental data.
- Experimentally, it was observed that the corrosion rates of carbon steel in the corrosive medium decreased with the addition of different concentrations of the inhibitor.
- A comparison of EMNQ2O inhibition efficiency in the salt solution (94.98%) is more electron deficient than in acid solution (81.40%). However the thermodynamic and kinetic parameters suggest that EMNQ2O has greater tendency to interact with the metal surface in (3.5% NaCl) solution than in (0.5M HCl) solution, and it is a very good inhibitor in both of them.

## Authors' declaration:

- Conflicts of Interest: None.
- We hereby confirm that all the Figures and Tables in the manuscript are mine ours. Besides, the Figures and images, which are not mine ours, have been given the permission for re-publication attached with the manuscript.
- Ethical Clearance: The project was approved by the local ethical committee in University of Baghdad.

## Authors' contributions statement:

M.A. contributed to samples preparation, performed the experiment calculations. R.K. devised the project, carried out the theoretical part with all its calculations (tables and figures), discussed all the results (experiment and theoretical), wrote the manuscript.

## References:

1. David A. Predicting the performance of organic corrosion inhibitors. Metals. 2017;7(553):1-8.
2. El-Bakri Y, Boudalia M, Echihi S, Harmaoui A, Sebhaoui J, Elmsellem H, et al. Performance and theoretical study on corrosion inhibition of new Triazolopyrimidine derivative for carbon steel in hydrochloric acid. J. Mat. Envir. Sci. 2017;8(2):378-388.
3. Yadav M, Kumar S, Behera D, Bahadur I, Ramjugernath D. Electrochemical and quantum chemical studies on adsorption and corrosion inhibition performance of quinoline-thiazole derivatives on mild steel in hydrochloric acid solution. Int. J. Electrochem Sci. 2014;9:5235–5257.
4. Louadi YE, Abrigach F, Bouyanzer A, Touzani R, El Assyry A, Zarrouk A, et al. Theoretical and Experimental Studies on the Corrosion Inhibition Potentials of Two Tetrakis Pyrazole Derivatives for Mild Steel in 1.0M HCl. Portug. Electrochim. Acta. 2017;35(3):159-178.
5. Kitagawa W, Tamura T. A Quinoline. antibiotic from rhodococcus erythropolis JCM 6824. J. Antibio. 2008;61(11): 680–682.
6. Kubba RM, Challoob DA. Hussen SM. Quantum mechanical and electrochemical study of new isatin derivative as corrosion inhibitor for carbon steel in 3.5 % NaCl. Int. J. Sci. Res. 2017; 6 (7);1656-1669.
7. GneDy PO, PALMER R, RoocEne H, Svrrn P. Isolation of aeromonass almonicidaS trains resistant to the Quinoline antibiotics. Bull. Eur. Ass. Fish parhol. 1987;7(2):43.
8. Fu HG, Li ZW, Hu XX, Si SY, You XF, Tang S, et al. Synthesis and biological evaluation of quinoline derivatives as a novel class of broad-spectrum antibacterial agents. Molecules. 2019 Jan;24(3):548..
9. Singh P, Srivastava V, Quraishi MA. Novel quinoline derivatives as green corrosion inhibitors for mild steel in acidic medium: electrochemical, SEM, AFM, and XPS studies. J. Mol. Liq. 2016;216:164–173.
10. Elyoussfi1 A, Dafali1 A, Elmsellem1 H, Bouzian Y, bouhfid R, Zarrouk1 A, et al. Some quinoline derivatives: Synthesis and comparative study towards corrosion of mild steel in 0.5M $H_2SO_4$. Der Phar. Chem. 2016;8(4):226-236.
11. Naik UJ, Jha PC, Lone MY, Shah RR, Shah NK. Electrochemical and theoretical investigation of the inhibitory effect of two Schiff bases of benzaldehyde for the corrosion of aluminium in hydrochloric acid. J. Mol. Str. 2016;1125:63–72.
12. Saha SK, Ghosh P, Hens A, Murmu NC, Banerjee P. Density functional theory and molecular dynamics simulation study on corrosion inhibition performance of mild steel by mercapto-quinoline Schiff base corrosion inhibitor. Physica E. 2015;66:332–341.
13. Sundaram RG, Sundaravadivelu M. Electrochemical and surface Investigation of quinoline-8-sulphonyl chloride as corrosion inhibitor for mild steel in acidic medium. Int J Chem Tech Res. 2016;9:527–539.
14. Luma SA, Rana AA, Rana SA, Mohammed RA, Redha IA. Synthesis of new 7-ethyl- 4-methy l-1-[(4-nitrophenyl)- amino]- 1H- quinolin- 2-one quinoline derivatives. Scientific International *Conference* , College of Science, AL-Nahrain Univesity. 2017;357:0–37.
15. Kubba RM, Al-Majidi SMH, Ahmed AH. Synthesis, characterization and quantum chemical studies of inhibition ability of novel 5-nitro isatin derivatives on

the corrosion of carbon steel in sea water. Iraq. J. Sci., 2019; 60(4):688-705.
16. Frisch MJ, Trucks GW, Schlegel HB, Scuseria GE, Robb MA, Cheeseman JR, et al. 01 Inc. Wallingford CT. 2009.
17. Kubba RM. Al-Majidi SMH, Ahmed AH. Synthesis, identification, theoretical and experimental studies for carbon steel corrosion inhibition in seawater for new urea and thiourea derivatives linkage to 5-nitro isatin moiety. Der Phar. Chem. 2018;10(7):86-99.
18. Lee C, Yang W, Parr RG. Development of the Colle-Salvetti correlation energy formula into a functional of the electron density. Phys. Rev. 1988;B 41:785-789.
19. Parr RG. Yang W. Density Functional Theory of Atoms and Molecules. 1ST Ed., Oxford University Press: New York, 1989.
20. Kubba RM, Alag AS. Experimental and theoretical evaluation of new quinazolinone derivative as organic corrosion inhibitor for carbon steel in 1M HCl solution. IJSR. 2017;6(6):1832-1843.
21. Duboscq J, Sabot R, Jeannin M, Refait Ph. Localized corrosion of carbon steel in seawater: Processes occurring in cathodic zones. Mat. Corr. 2019;70(6):941-1140.
22. Fleming I. Frontier Orbitals and Organic Chemical Reactions. John Wiley and Sons, NewYork, 1976.
23. Koopmans T. Über die Zuordnung von Wellenfunktionen und Eigenwerten zu den Einzelnen Elektronen Eines Atoms. Physica. 1933;1:104-113.
24. Parr RG, Donnelly RA, Levy M, Palke WE. Empirical evaluation of chemical hardness. J. Chem. Phys. 1978;68:3801-3807.
25. Kubba RM, Mohammed M. Theoretical studies of corrosion inhibition efficiency of two new N-phenyl-ethylidene-5-bromo isatin derivatives. Iraq. J. Sci. 2016;57(2B):1041-1051.
26. Singh A, Ansari KR, Lin Y, Quraishi MA, Lgaz H, Chung IM. Corrosion inhibition performance of imidazolidine derivatives for J55 pipeline steel in acidic oilfield formation water: Electrochemical, surface and theoretical studies. J. Taiw. Inst. Chem. Eng. 2019;95:341-356.
27. Kubba RM, Mohammed M. Synthesis, identification, theoretical and experimental studies of carbon steel corrosion inhibition in seawater by some new diazine derivatives linked to 5-nitroisatin moiety. Iraq. J. Sci. 2018;59(3B):1347-1365.
28. Anbarasi CM, Rajendran S. Surface protection of carbon steel by butanesulphonic acid-zinc ion system. Res. J. Chem. Sci. 2012;2(12):21-26.
29. Liu Y, Wang Z, Wei Y. Influence of seawater on the carbon steel initial corrosion behavior. Int. J. Electrochem. Sci.2019;14:1147–1162.
30. Ahmed AH, Al-Majidi SMH, Kubba RM. Surface protection of carbon steel by butane sulphonic acid-zinc ion system. J. Glob. Pharma Tech. 2018;10(05):369-383.

# دراسة نظرية وتجريبية لسلوك تآكل سطح حديد الصلب الكربوني في 3.5% كلوريد الصوديوم و 0.5M حامض الهيدروكلوريك عند تراكيز مختلفة من مشتق الكوينولين-2-اون

**رحاب ماجد كبة** **مصطفى علاء محمد**

قسم الكيمياء كلية العلوم، جامعة بغداد، بغداد، العراق

**الخلاصة:**

تم اجراء دراسة نظرية وتجريبية على حماية تآكل سطح حديد الصلب الكربوني عند تراكيز مختلفة من مشتق (الكوينولين-2-اون) الذي يحمل الاسم: 7-Ethyl-4-methyl-1-[(4-nitro-benzylidene)-amino]-1H-quinolin-2-one (EMNQ2O). من الناحية النظرية، تم استخدام نظرية دالة الكثافة (DFT) عند المستوى (B3LYP) 6-311++G (2d,2p) لحساب التركيب الهندسي والخصائص الفيزيائية ومعايير كفاءة التثبيط الكيميائية، مع مواقع الامتزاز الفعالة من أجل التنبؤ بمعرفة المواقع المحتملة للهجمات النكليوفيلية والالكتروفيلية في الفراغ و في اثنين من المذيبات (DMSO و $H_2O$)، كل ذلك عند الاشكال الهندسية التوازنية. من الناحية التجريبية، تمت دراسة كفاءاة التثبيط (IE%) في محلولي (3.5% من NaCl) و (0.5M HCl) باستخدام قياسات الاستقطاب المجهادي. أظهرت النتائج أن كفاءة التثبيط (IE%) في المحلول الملحي (**94.98%**) أكبر مما هي في المحلول الحامضي (**81.40%**). المعلمات الديناميكية الحرارية التي تم الحصول عليها تدعم آلية الامتزاز الفيزيائي وأن امتزازه على سطح حديد الصلب الكربوني يطيع ايزوثيرم امتزاز لنكماير isotherm Langmuir. وتمت دراسة التغيرات السطحية لحديد الصلب الكربوني باستخدام تقنيتي الفحص المجهري للإلكترون (SEM) والفحص المجهري للقوة الذرية (AFM).

**الكلمات المفتاحية :-** تثبيط التآكل، DFT، الكوينولين، المعلمات الديناميكية الحرارية.